Bulletin of the
Seismological Society of America

Vol. 79 August 1989 No. 4

TELESEISMIC AND STRONG-MOTION SOURCE SPECTRA FROM TWO EARTHQUAKES IN EASTERN TAIWAN

By Lorraine J. Hwang and Hiroo Kanamori

Abstract

The 20 May and 14 November 1986 Hualien earthquakes occurred in a seismically active region of Taiwan. Locally determined focal mechanisms and aftershock patterns from the Taiwan Telemetered Seismographic Network indicate that both earthquakes occurred on steeply dipping reverse faults that trend NNE. This agrees with teleseismic first-motion data for the May event but not for the November event. This discrepancy is due to a moderate foreshock before the November event. Surface-wave analysis gives a solution for the November event of: dip 57°, rake 100°, and strike 43°, which is similar to the locally reported focal mechanism. The seismic moment of the November event is $M_0 = 1.7 \times 10^{27}$ dyne-cm and the magnitudes determined from WWSSN data are $\hat{m}_b = 6.4$, $M_s = 7.3$. Teleseismic source spectra show that the two events also have similar spectral signatures above 0.15 Hz. Reference acceleration spectra are computed from the average teleseismic source spectra and compared to the averaged acceleration spectra computed from strong-motion stations for both events. Correlations between the spectral amplitudes of the strong-motion spectra obtained from the main portion of the SMART 1 array and the teleseismically estimated reference spectra are poor above 0.2 Hz. Data from the hard-rock site situated outside of the basin indicates that amplification of the ground motion between 0.17–1.7 Hz is due to the alluvial valley where the SMART 1 array is located. The amplitude of the observed spectrum is five times the reference spectrum at the hard-rock site. This is consistent with similar observations from the 1985 Michoacan and 1983 Akita-Oki earthquakes. The analysis of these and more teleseismic and strong-motion records will lead to a better understanding of the relationship between their spectra.

Introduction

The determination of strong ground motion for large earthquakes is a fundamental problem in earthquake engineering. To design structures that withstand large earthquakes, an engineer must consider the spectral content as well as duration of an expected event. Only recently have near-field strong-motion data become available for large earthquakes and efforts begun to understand the regional variations of the source spectra.

Three factors determine the strong ground motion spectra: the source, path, and site effect. Since the source spectra at periods between 1 to 20 sec can be reliably determined from Global Digital Seismic Network (GDSN) data, path and site effects in the epicentral region can be evaluated by comparing teleseismic and strong-motion data. To do this, it is necessary to study those events for which both strong motion and teleseismic recordings are available. One approach to estimating path and site effects is the use of numerical techniques such as the finite element or difference method to model the local structure. However, the local structure is not always known well enough for such modeling. In addition, these techniques do

not accommodate large source-receiver distances very well in the frequency range of interest.

In this paper, we take an alternative, empirical approach. We compare the observed strong-motion spectra with the teleseismically determined source spectra assuming that the strong-motion data are recorded on the surface of a uniform half-space. In most cases, this is a simplification of the real situation. However, any discrepancies between the observed and estimated spectra can be interpreted as due to the combined path and site effect. Differences will vary as a function of distance and may also depend on source region and earthquake magnitude. The accumulation of data for a sufficiently large number of events to establish general relationships for different sites will enable the estimation of strong ground motion spectra for different earthquakes. Houston and Kanamori (unpublished manuscript) used this approach to study the 1985 Michoacan, Mexico, and 1983 Akita-Oki, Japan, earthquakes. Two recent earthquakes in eastern Taiwan were well recorded at both teleseismic stations and a local strong-motion array and provide an excellent data set for this study.

The island of Taiwan is located in a young, active orogenic belt on the boundary between the Eurasian and Philippine Sea plates. Collision along this boundary has formed belts of deformed NNE trending Tertiary geosynclinal sediments and metamorphics paralleling the axis of the island. Near Hualien, the boundary between the two plates changes from the south from a northeast-trending oblique slip

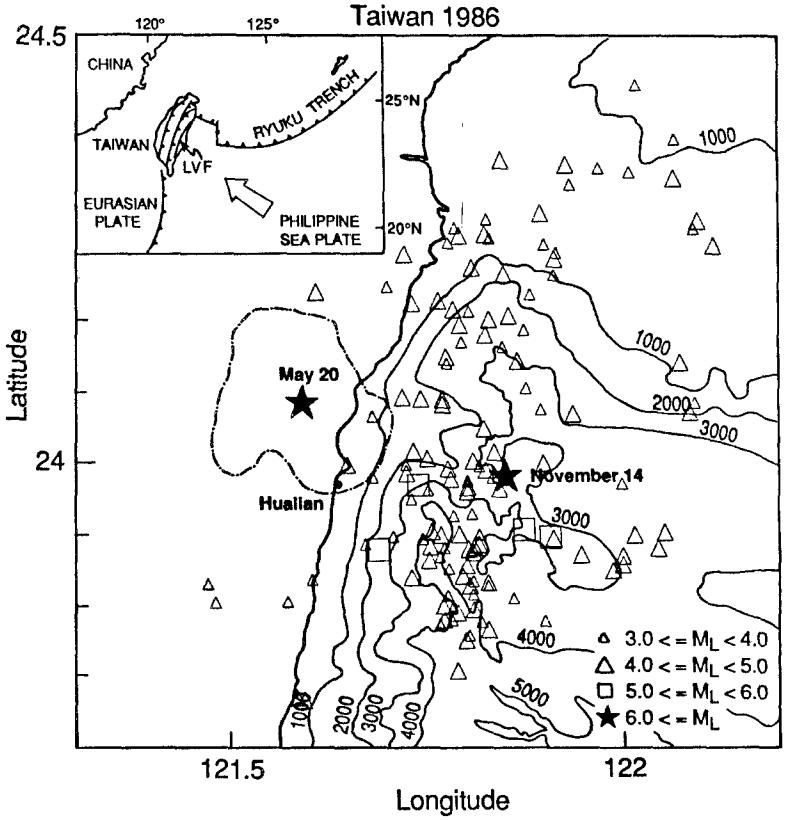

FIG. 1. Inset shows the regional tectonics in the Taiwan region (after Ho, 1986). Symbols used are noted in the figure. LVF is the Longitudinal Valley fault. Outlined with dot-dashed lines is the aftershock region for the 20 May 1986 earthquake. Also shown is the 14 November 1986 earthquake along with the aftershocks from 14 to 30 November 1986 preliminarily located by TTSN.

transform fault, the Longitudinal Valley fault (LVF), to an east-west trending thrust fault with the Philippine Sea plate subducting northward under the Eurasian plate along the Ryuku trench (Fig. 1). Two major earthquakes in the Hualien region in 1951 were accompanied by reverse oblique slip on the LVF. The two earthquakes studied here, the 20 May 1986 (05h 25m 46.9s UTC, 24.125°N, 121.619°E, h = 19 km, M_s = 6.4, NEIC) and the 14 November 1986 (21h 20m 10.5s UTC, 23.961°N, 121.836°E, h = 34 km, M_s = 7.8, NEIC) events, both occurred along the very active eastern coast of Taiwan near the city of Hualien. These events were recorded both worldwide and by the SMART 1 accelerograph network on the Lanyang Plain near Lotung, Taiwan. The availability of high-quality digital data sets, the similarity of their focal mechanisms, and their close proximity to each other provide a good opportunity to study and compare the strong motion and teleseismic spectra for events in this region.

20 May 1986 Hualien Earthquake

Seismicity and source parameters of the May 1986 event (event 1) have been studied using data from the local array, the Taiwan Telemetered Seismographic Network (TTSN), as well as temporary seismic stations deployed soon after the main shock (Chen and Wang, 1986; Liaw *et al.*, 1986; Yeh *et al.*, 1988) and are briefly reviewed here. The TTSN relocated the hypocenter to 24.082°N, 121.592°E, h = 15.8 km, and M_L = 6.5 ($M_o = 2.6 \times 10^{25}$ dyne-cm, NEIC). First motions from local data constrained the focal mechanism to: dip 60°, rake 90°, and strike 35° (Chen and Wang, 1986). This is in good agreement with the teleseismic first motions we determined from GDSN and WWSSN data (Fig. 2).

Aftershock activity associated with the main shock occurred within a small area on two parallel, eastward, steeply dipping thrust faults. Activity migrated from the eastern to the western fault zone. Both structures are consistent with the regional tectonic setting. Aftershocks immediately following the main shock, which were relocated by Liaw *et al.* (1986) using high-quality local data, locate to the northwest of the main shock and above the hypocenter located at 16 km depth. This spatial

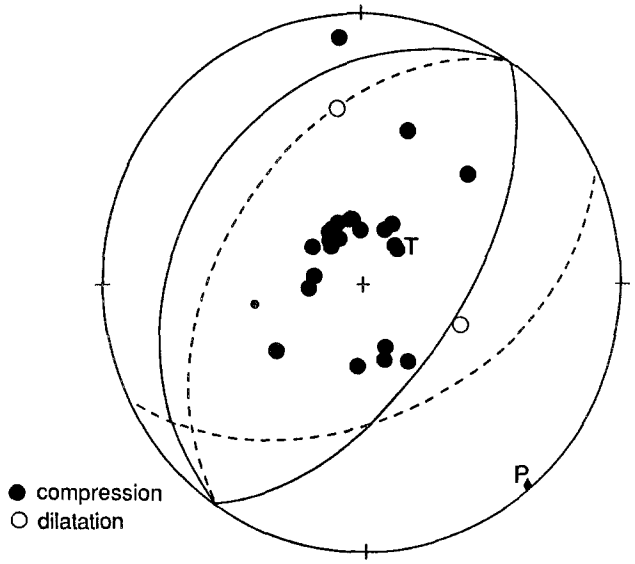

FIG. 2. Focal mechanisms shown here and in subsequent plots are lower hemisphere projections. The solid lines show the locally determined focal mechanism for the 20 May 1986 Hualien earthquake (Chen and Wang, 1986). The dashed line shows the Harvard centroid moment tensor (CMT) solution (NEIC). Large symbols are good quality picks and small symbols, poor quality.

relation between the main shock and the aftershocks suggests that the rupture initiated at 16 km depth and propagated unilaterally upward to the northwest.

14 November 1986 Hualien Earthquake

Seismicity and source parameters of the November 1986 event (event 2) are studied here using WWSSN, GDSN, *Preliminary Determination of Epicenter* (PDE), and TTSN data. The locally determined hypocenters of the main shock (23.992°N, 121.833°E, $h = 13.9$ km, $M_L = 6.8$; Yeh *et al.*, 1988) and aftershocks form a NNE-trending band of seismicity just offshore Hualien. The aftershocks are primarily concentrated in the upper 15 km of the crust but extend down to a depth of 37 km. Activity appears to be confined within the nonsubducted portion of the Philippine Sea plate which is 50 km thick in this region (Tsai *et al.*, 1977). The aftershock region for this event adjoins that from event 1, which lies immediately to the west (Fig. 1).

Source Parameters

Analysis of teleseismic first motions conflicts with the locally determined solution of strike 38° and dip 58° (Yeh *et al.*, 1988) (Fig. 3). This is due to a moderate foreshock ($m_b = 5.4$) occurring 5 sec before the main event. This foreshock can be identified on most WWSSN records. However, overall data quality for the body waves is poor. A more robust determination of the focal mechanism is made by inverting the Rayleigh and Love waves recorded by the GDSN stations over a period range of 180 to 285 sec using a centroid moment tensor code (CMT) written by Kawakatsu and Kanamori (1989), which is similar to that developed by Dziewonski *et al.* (1981). Three component data from 7 stations (ANMO, BCAO, HON, KONO, NWAO, SNZO, WMQ) are used to invert Rayleigh and Love-wave phases R1-R3 and L1-L3, respectively. The preferred fault parameters for the best-fit double couple in the CMT inversion are strike 43°, dip 57°, rake 100° (strike 33°, dip 57°, rake 92°, HRV), and a moment of $M_o = 1.72 \times 10^{27}$ dyne-cm. This mechanism is consistent with the structural trends in this region. The amplitudes of body and

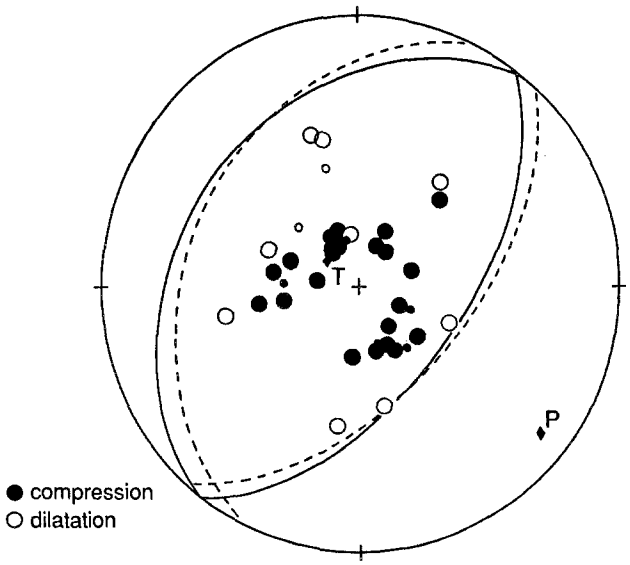

FIG. 3. The solid line shows the locally determined focal mechanism for the 14 November 1986 Hualien earthquake (Yeh *et al.*, 1988). The dashed line shows our CMT solution. Symbols are the same as in Figure 2.

surface waves from short-period vertical component WWSSN instruments yield magnitudes of $\hat{m}_b$ = 6.4 (19 stations, σ = 0.29) ($\hat{m}_b$ is defined after Houston and Kanamori, 1986) and M_s = 7.3 (11 stations, σ = 0.40). Note that this estimate of M_s is substantially less than the reported NEIC value.

The source-time function and rupture pattern are determined by simultaneous inversion of the body waves following Kikuchi and Fukao (1985). We invert the first 60 sec of the body wave from four long-period vertical component WWSSN stations and four vertical component GDSN stations combining short- and long-period data to yield a WWSSN-type instrument response. The fault plane is determined by the extent of the aftershock zone within the first 24 hours of the main shock. The focal mechanism is constrained by the surface-wave data. Distance and time are relative to the hypocenter and origin time, respectively, determined from local data.

Total moment release for our model is 1.9 × 10^{27} dyne-cm. Figure 4 shows the resulting synthetics (dashline), data (solid line) and source-time function. Moment release between 0 and 5 sec is associated with the foreshock. It reaches its peak between 5 and 14 sec followed by a smaller moment releasing episode of long duration between 20 and 32 sec. Most of the moment release occurs close to the epicenter (Fig. 5). While the long-period data cannot discriminate between individual point sources, modeling using different parameterizations for the point sources indicates that the source-time function and position of major moment releasing subevents are robust.

Teleseismic and Strong-Motion Source Spectra

Source spectra for the two events are calculated between the periods of 1 to 20 sec from GDSN records using the method of Houston and Kanamori (1986). In their method, the spectrum is corrected for instrument response, geometrical

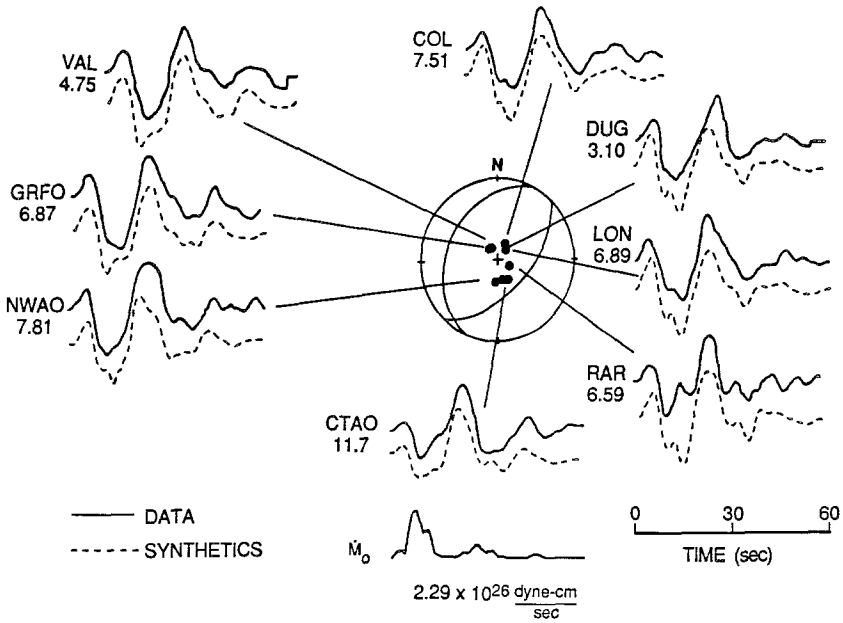

FIG. 4. Comparison of actual (solid line) and synthetic (dashed line) seismograms from the body-wave inversion. Peak amplitudes for the data in cm is given below each station for a long period WWSSN instrument with a magnification of 1500. The synthetics at each station are plotted to the same scale as the data. The focal mechanism and stations used in the inversion and the resulting source-time function are shown. The peak moment release rate for the source time function is 2.29 × 10^{26} dyne-cm/sec.

spreading, radiation pattern, and the free-surface receiver effect. The density and P-wave velocity within the crust is taken here to be 2.8 gm/cm^3 and 6.5 km/sec, respectively. Attenuation is corrected assuming t^* (travel time divided by the path average Q) = 0.7 sec. The average moment rate and acceleration spectra are computed from six short-period teleseismic P-wave seismograms for event 1, and 7 for event 2. The overall shape of the teleseismic spectrum of the two events is consistent with the ω^{-2} model and both displacement spectra have a similar shape above 0.15 Hz (Fig. 6). However, between 0.05 and 0.15 Hz, the displacement spectrum for the first event drops considerably in amplitude. This difference is more clearly seen in the acceleration spectra of the two events (Fig. 6b). Differences in the spectra may reflect differences in the rupture pattern between the two events. Unfortunately, we could not determine the rupture pattern of event 1 because of its relatively small size.

The strong-motion spectra are computed from the data obtained from the SMART 1 array. The main portion of the SMART 1 array is comprised of 37 stations in 3 concentric rings with radius of 0.2, 1.0, and 2.0 km, respectively. Two external stations are located at a distance of 2.8 and 4.8 km south of the central station of the main array. The array is situated 70 and 77 km north from the two events, respectively, in an alluvial valley of recent age. The water table is either

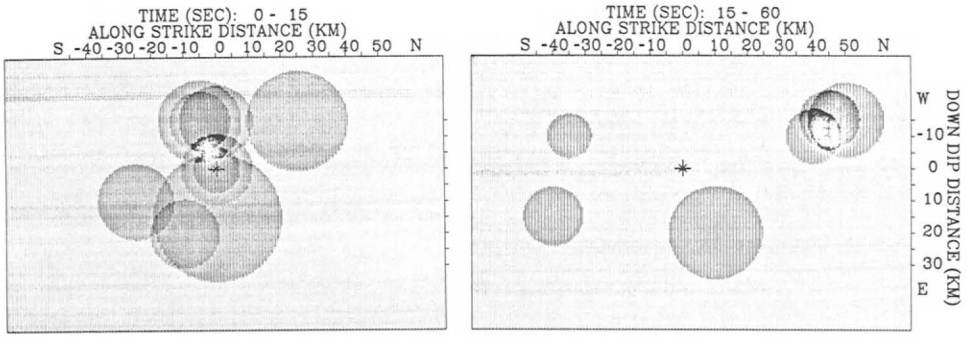

FIG. 5. Time slices of the spatial distribution of moment release projected onto the fault surface. The radius of each circle is proportional to the seismic moment of the point source it represents. The asterisk marks the hypocenter.

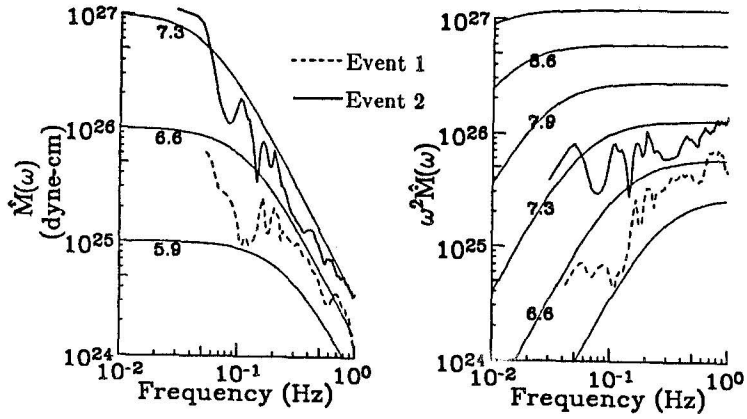

FIG. 6. (a) Average moment rate spectra and (b) average acceleration spectra from teleseismic GDSN stations for event 1 (dashed line) and event 2 (solid line). Theoretical spectra for an ω^{-2} model are shown by thin lines.

near or at the ground surface (Abrahamson *et al.*, 1987). Figure 7 shows the average strong-motion spectra for the two events. Figure 8 shows the spectrum for the hard rock station E02 which triggered only for event 2.

As shown above, the two events have similar focal mechanisms and source locations but very different magnitudes. The difference of 0.3 in M_L between the two events is consistent with the difference of about a factor of 2 in the moment-rate spectrum at 1 Hz (Fig. 6). However, the amplitude of the strong-motion spectrum at 1 Hz for event 1 is about the same as that for event 2 (Fig. 7). In addition, the overall shape of the acceleration spectrum determined from the strong-motion records is very different between the two events. This difference is due to the difference in magnitude which causes a spectral shift and is probably also due to the difference in the epicentral locations of the two events with respect to the Lanyang Plain. This suggests the importance of the source-site geometry for amplification of near-field strong ground motions. Although the effect of difference

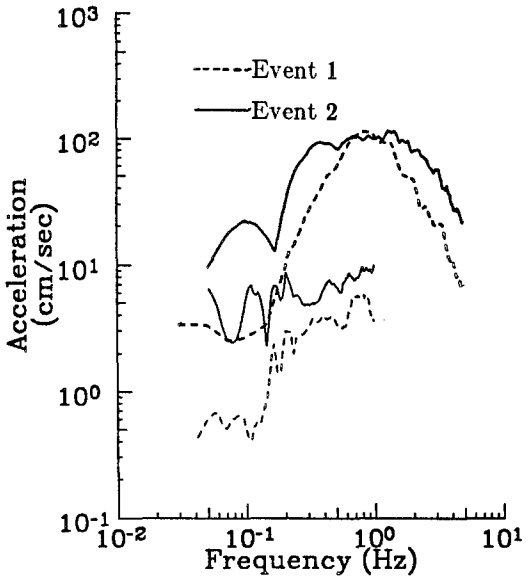

FIG. 7. Averaged strong-motion spectra from the SMART 1 array and teleseismically estimated reference spectra for both events. Strong-motion spectra are shown in thick lines and teleseismic spectra with thin lines. Event 1 is given with dashed lines and event 2 with solid lines.

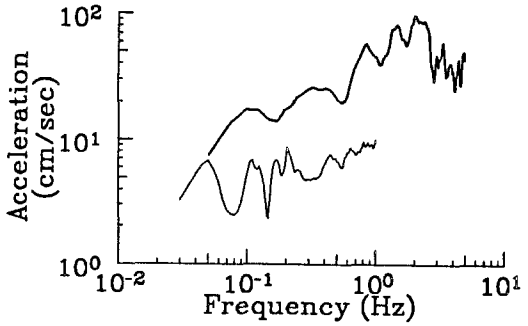

FIG. 8. Comparison of strong-motion and reference spectra between site E02 and event 2. Strong-motion spectra are shown in thick lines and teleseismic spectra with thin lines.

in the epicentral location is small for teleseismic stations, it can be significant for local stations.

The observed acceleration spectra cannot be directly compared with the source spectra determined from teleseismic data. Since our purpose is to estimate path and site effects, we want to compare the observed spectra with spectra that would have been observed from a simple structural model that has no significant path and site effects. Hence, following Houston and Kanamori (unpublished manuscript) we assume that strong ground motions consist of far-field S waves from a point source recorded on the surface of a uniform half-space, and compute the acceleration spectrum from the point source spectrum obtained from teleseismic data. The spectra are corrected for the free-surface effect for SH waves and the S radiation pattern averaged over the entire focal sphere. $Q = 300$ is assumed. In the half-space, the S-wave velocity is assumed to be $\beta = 3.8$ km/sec and density, $\rho = 2.8$ g/cm^3. The distance between the source and receiver is 70 and 77 km for event 1 and event 2, respectively. The spectrum thus calculated is called the reference spectrum. The reference spectrum is not a direct estimate of the acceleration spectrum at a specific site, but is a standard against which the observed spectrum is compared. Any difference from the reference spectrum is attributed to path and site effects.

A finite source was not considered. For event 1, the low magnitude of the event indicates that the point source approximation is reasonable. For event 2, the point source approximation is applied since most of the moment release occurred within the first 15 sec (Fig. 4) within a small region close to the nucleation point (Fig. 5).

Comparison between the reference acceleration spectra estimated from teleseismic data and the strong-motion spectra (Fig. 7) shows that beginning approximately at 0.2 Hz the strong-motion spectra start to differ substantially from the reference spectra. The amplitude ratio of the strong-motion spectrum to the reference spectrum increases with increasing frequency. For event 1, the strong-motion spectrum at 0.2 Hz is three times the amplitude of the reference spectrum. This ratio increases to 20 at 1 Hz. Similarly, for event 2 the strong-motion spectrum at 0.2 Hz is four times the amplitude of the reference spectrum and increases to 10 at 1 Hz.

Site Effect

The spectral amplitudes of the strong motion records in this study are 10 to 20 times larger than the reference spectra computed from teleseismic data. This discrepancy is larger than those found for other large subduction zone events. Examples from the 1985 Michoacan and 1983 Akita-Oki earthquakes at similar distances (Houston, 1986) do not exhibit such large discrepancies as those from the Hualien events. For these events, the observed strong-motion spectrum is about two to five times the amplitude of the reference spectrum.

Site amplification due to sediment-filled basins has been studied by many authors. Both analytical (Aki and Larner, 1970; Wong and Trifunac, 1974; Bard and Bouchon, 1980; Bravo *et al.*, 1988) and finite-difference and finite-element (Boore *et al.*, 1971; Joyner, 1975; Joyner and Chen, 1975; Vidale and Helmberger, 1988) techniques have been used to study the variations in amplitudes across sediment-filled basins. Amplitudes vary with the position of the receiver with respect to the geometry of the basin. Surface amplitudes also depend on the thickness of the sedimentary layers, impedance contrast between the layers, and the frequency and angle of incidence of the incoming wave. Analytical modeling suggests that basin effects can cause amplitude variations of up to 7 times that of an equivalent horizontal layer model (Wong and Trifunac, 1974). Larger amplitude ratios with

respect to rock sites are expected and have been observed. King and Tucker (1984) observed that motions on the sediments of the Chusal Valley, USSR, are up to 10 times larger than the nearby rock sites. Vidale and Helmberger (1988) also observed and modeled this effect for the 1971 San Fernando, California, earthquake.

The above studies show that we can expect site amplifications produced by the alluvial valley where the SMART 1 array is situated. This effect is observed in this study and by Bolt and Chiou (1987). Bolt and Chiou (1987) observed for event 2 that the peak accelerations in the valley were up to 1.7 times and peak velocities up to 3.2 times that of the rock site. In our study, this is illustrated by comparisons of the acceleration spectrum of the rock site to the alluvial site and to the reference spectrum. Comparison of the spectral amplitudes between the external hard-rock site, E02, and the soft rock sites show that the spectral amplitude at E02 is about three times lower than that from the soft-rock sites for event 2 at frequencies between 0.17 and 1.7 Hz (Fig. 8). Unfortunately, E02 did not trigger for event 1 so the same comparison cannot be made for that event. The importance of site effects is further underscored when site E02 is compared to the reference spectrum. The overall spectral shape of E02 more closely matches the reference spectrum for event 2 than the spectrum from the main portion of the array. In addition, the observed spectrum from site E02 is five times the amplitude of the reference spectrum, which is consistent with observations by Houston (1986).

Conclusions

Two recent damaging earthquakes, the 20 May 1986 and 14 November 1986 Hualien earthquakes, provided a good opportunity to compare the near-field acceleration spectra and the source spectra determined from teleseismic data. Both events occurred in the same region of eastern Taiwan; epicenters are approximately 25 km apart; and both occurred within a short time of each other. The focal mechanisms of both events indicates faulting along NNE-trending, steeply eastward dipping, reverse faults.

Acceleration spectra from the two events are compared with the reference spectrum computed from the teleseismically determined source spectrum. We define the reference spectrum to be the acceleration spectrum computed from the point source spectrum assuming a uniform half-space. The reference spectrum is a standard to be used in comparison to the observed acceleration spectra. Differences between the two spectra can be interpreted as due to path and site effects. The results obtained from the SMART 1 data clearly demonstrate the importance of site effects. The average amplitude spectrum computed from the main portion of the array situated on alluvium is about 20 times larger than the amplitude of the reference spectrum. For the 14 November 1986 Hualien earthquake, the ratio of the spectral amplitude observed at a hard-rock site to the reference spectrum agrees well with those observed for the 1985 Michoacan and 1983 Akita-Oki earthquakes observed under similar conditions (Houston, 1986). These results suggest that if similar comparisons are made for events in different tectonic provinces, teleseismically determined source spectra may be eventually used to estimate strong ground motions for different tectonic regions.

Acknowledgments

We thank the personnel from the WWSSN stations and the USGS for making their data available to us. Thanks to Frances Wu and Kuo-Liang Wen who kindly shared aftershock data from TTSN with us and to Heidi Houston and Y.T. Yeh who made preprints available. The SMART 1 Array data were made

available by Bruce Bolt through the Seismographic Station of the University of California at Berkeley and the Institute of Earth Sciences of the Academia Sinica in Taipei. This research was supported by USGS Grant No. 14-08-0001-G1356 NSF EAR-86-18189 and an NSF Graduate Fellowship. Contribution No. 4662, Division of Geological and Planetary Sciences, California Institute of Technology, Pasadena, CA 91125.

REFERENCES

Abrahamson, N. A., B. A. Bolt, R. B. Darragh, J. Penzien, and Y. B. Tsai (1987). The SMART 1 accelerograph array (1980–1987): a review, *Earthquake Spectra* **3,** 263–281.

Aki, K. and K. L. Larner (1970). Surface motion of a layered medium having an irregular interface due to incident plane SH waves, *J. Geophys. Res.* **75,** 933–954.

Bard, P.-Y. and M. Bouchon (1980). The seismic response of sediment-filled valleys. Part 1. The case of incident *SH* waves, *Bull. Seism. Soc. Am.* **70,** 1263–1286.

Bolt, B. and S.-J. Chiou (1987). Strong motion array analysis of the November 14, 1986 Taiwan earthquake (abstract), *XIX General Assembly of the International Union of Geodesy and Geophysics* **1,** 303.

Boore, D. M., K. L. Larner, and K. Aki (1971). Comparison of two independent methods for the solution of wave scattering problems: response of a sedimentary basin to incident *SH* waves, *J. Geophys. Res* **76,** 558–569.

Bravo, M. A., F. J. Sanchez-Sesma, and F. J. Chavez-Garcia (1888). Ground motion on stratified alluvial deposits for incident *SH* waves, *Bull. Seism. Soc. Am.* **78,** 436–450.

Chen, K. C. and J. H. Wang (1986). The May 20, 1986 Hualien, Taiwan earthquake and its aftershocks, *Bull. Inst. Earth Sci., Academia Sinica* **6,** 1–13.

Dziewonski, A. M., T. A. Chou, and J. H. Woodhouse (1981). Determination of earthquake source parameters from waveform data for global and regional seismicity, *J. Geophys. Res.* **86,** 2825–2852.

Ho, C. S. (1986). A synthesis of the geologic evolution of Taiwan, *Tectonophysics* **125,** 1–16.

Houston, H. (1986). Source characteristics of large earthquakes at short periods, *Ph.D. Thesis* California Institute of Technology, Pasadena, California 129 pp.

Houston, H. and H. Kanamori (1986). Source spectra of great earthquakes: teleseismic constraints on rupture process and strong motion, *Bull. Seism. Soc. Am.* **76,** 19–42.

Joyner, W. B. (1975). A method for calculating nonlinear seismic response in two dimensions, *Bull. Seism. Soc. Am.* **65,** 1337–1357.

Joyner, W. B. and A. T. F. Chen (1975). Calculation of nonlinear ground motion response in earthquakes, *Bull. Seism. Soc. Am.* **65,** 1315–1336.

Kawakatsu, H. and H. Kanamori (1989). Centroid single force inversion of seismic waves generated by landslides (submitted for publication).

Kikuchi, M. and Y. Fukao (1985). Iterative deconvolution of complex body waves from great earthquakes—the Tokachi-Oki earthquake of 1968, *Phys. Earth. Planet. Interiors* **37,** 235–248.

King, J. L. and B. E. Tucker (1984). Observed variations of earthquake motion across a sediment-filled valley, *Bull. Seism. Soc. Am.* **74,** 137–151.

Liaw, Z. S., C. Wang, and Y. T. Yeh (1986). A study of aftershocks of the 20 May 1986 Hualien earthquakes, *Bull. Inst. Earth Sci., Academia Sinica* **6,** 15–27.

Tsai, Y. B., T. L. Teng, J. M. Chiu, and H. L. Liu (1977). Tectonic implications of the seismicity in the Taiwan region, *Mem. Geol. Soc. China* **2,** 13–41.

Vidale, J. E. and D. V. Helmberger (1988). Elastic finite-difference modeling of the 1971 San Fernando, California earthquake, *Bull. Seism. Soc. Am.* **78,** 122–141.

Wong, T. L. and M. D. Trifunac (1974). Surface motion of a semi-elliptical alluvial valley for incident plane *SH* waves, *Bull. Seism. Soc. Am.* **64,** 1389–1408.

Yeh, Y. T., C. L. Tsai, K. C. Chen, K. L. Wen (1988). An investigation of two destructive Hualien earthquakes in 1986 in the Taiwan area, *Bull. Inst. Earth Sci., Academia Sinica* (in press).

SEISMOLOGICAL LABORATORY
CALIFORNIA INSTITUTE OF TECHNOLOGY
PASADENA, CALIFORNIA 91125

Manuscript received 4 August 1988